Pressure studies of the quantum critical alloy $Ce_{0.93}Yb_{0.07}CoIn_5$

Y. P. Singh,[1,*] D. J. Haney,[1,*] X. Y. Huang,[1] B. D. White,[2] M. B. Maple,[2] M. Dzero,[1] and C. C. Almasan[1]

[1]*Department of Physics, Kent State University, Kent, Ohio 44242, USA*

[2]*Department of Physics, University of California at San Diego, La Jolla, California 92903, USA*

(Received 19 November 2014; revised manuscript received 22 April 2015; published 11 May 2015)

Here we present our experimental and theoretical study of the effects of pressure on the transport properties of the heavy-fermion alloy $Ce_{1-x}Yb_xCoIn_5$ with actual concentration $x \approx 0.07$. We specifically choose this value of ytterbium concentration because the magnetic-field-induced quantum critical point, which separates the antiferromagnetic and paramagnetic states at zero temperature, approaches zero, as has been established in previous studies. Our measurements show that pressure further suppresses quantum fluctuations in this alloy, just as it does in the parent compound $CeCoIn_5$. In contrast, the square-root temperature-dependent part of resistivity remains insensitive to pressure, indicating that the heavy quasiparticles are not involved in the inelastic scattering processes leading to such a temperature-dependent resistivity. We demonstrate that the growth of the coherence temperature with pressure, as well as the decrease of the residual resistivity, can be accurately described by employing the coherent potential approximation for a disordered Kondo lattice.

DOI: 10.1103/PhysRevB.91.174506 PACS number(s): 71.10.Hf, 71.27.+a, 74.70.Tx

I. INTRODUCTION

Since their discovery almost thirteen years ago [1,2], the family of 115 materials has provided an impactful experimental and theoretical playground for studying fundamental quantum phenomena, such as magnetism and superconductivity, in strongly interacting electronic systems [3]. In particular, the physical and structural properties of these materials have not only helped to further develop the concepts of quantum phase transitions and non-Fermi liquids, but have also motivated theoretical studies of exotic mechanisms for unconventional superconductivity. Moreover, it has been shown recently that f-orbital compounds may host topologically nontrivial electronic states [4–9]. Whether the 115-based alloys can host topologically nontrivial superconductivity remains an open question, which provides an additional motivation for both experimental and theoretical communities to study the normal and superconducting properties of these systems in greater detail.

Heavy-fermion alloys $Ce_{1-x}Yb_xCoIn_5$—members of the 115 family of compounds—possess a number of intriguing and often counterintuitive physical properties: (i) upon an increase in the concentration of ytterbium atoms, the critical temperature of the superconducting transition (T_c) decreases only slightly compared to other rare-earth substitutions [10,11] and superconductivity persists up to the nominal concentration $x_{\rm nom} \approx 0.75$; (ii) the value of the out-of-plane magnetic field (H) corresponding to the antiferromagnetic (AFM) quantum critical point (QCP) approaches zero as $x_{\rm nom} \to 0.2$ [12]: (iii) there is a crossover in the temperature (T) dependence of resistivity (ρ_a) measured along the a axis: the resistivity has a $\sqrt{T}$ dependence, except at the lower doping levels ($x_{\rm nom} \leqslant 0.2$) where it exhibits an additional linear-in-T contribution [13], i.e.,

$$\rho_a(x,T) = \rho_{a0}(x) + A(x)T + B(x)\sqrt{T} \qquad (1)$$

with $\rho_{a0}(x) \propto x_{\rm nom}(1 - x_{\rm nom})$ (in accord with Nordheim law) [14,15], $B(x) \to 0$ as $x_{\rm nom} \to 0$ and $A(x) \to 0$ as $x_{\rm nom}$ is gradually increased from zero to $x_{\rm nom} \approx 0.2$; (iv) there is a drastic Fermi-surface reconstruction for $x_{\rm nom} \approx 0.55$, yet T_c remains weakly affected [16]. More recently, penetration depth measurements [17] have shown the disappearance of the nodes in the superconducting order parameter for $x_{\rm nom} \geqslant 0.2$.

The emergent physical picture, which describes the physics of these alloys is based on the notion of coexisting electronic networks coupled to conduction electrons: one is the network of cerium ions in a local moment regime, while the other consists of ytterbium ions in a strongly intermediate-valence regime [18,19]. This picture is supported by recent extended x-ray absorption fine structure spectroscopic measurements [20], as well as photoemission, x-ray absorption, and thermodynamic measurements [21,22]. Moreover, our most recent transport studies [13] are generally in agreement with this emerging physical picture. In particular, for $x_{\rm nom} \approx 0.6$ we observe the crossover from coherent Kondo lattice of Ce to coherent behavior of Yb sublattice, which is in agreement with recent measurements of the De Haas-van Alphen effect [16], while superconductivity still persists up to $x_{\rm nom} \approx 0.75$ of ytterbium concentration. Nevertheless, it remains unclear which of the conduction states—strongly or weakly hybridized—of the stoichiometric compound contribute to each network.

In order to get further insight into the physics of the $Ce_{1-x}Yb_xCoIn_5$ alloys, we study the transport properties under applied magnetic field and pressure for the alloy with actual concentration $x_{\rm act} \approx 0.07$. One of our goals is to clarify the origin of the square-root temperature dependence of resistivity and to probe the contribution of the heavy quasiparticles to the values of $A(x)$ and $B(x)$ [see Eq. (1)]. To address this issue, we study the changes in the residual resistivity and the coefficients A and B with pressure. Our results show that while both the residual resistivity and the coefficient A decrease with pressure, B shows very weak pressure dependence. This indicates that the AFM quantum fluctuations are suppressed with pressure and that the light quasiparticles involved in the scattering mechanism that gives the $\sqrt{T}$ dependence originate from the electrons from the small Fermi surface that hybridize

[*]These authors have contributed equally to this work.

with Yb ions. We find that the Kondo lattice coherence and the superconducting critical temperature increase with pressure in accord with general expectations [13,23]. We also study theoretically the properties of a disordered Kondo lattice in which the disorder ions are magnetic. Within the picture of the single conduction band, we show that the presence of the magnetic ions has little effect on the dependence of the residual resistivity and the Kondo lattice coherence temperature on pressure. Our theoretical results are in good agreement with our experimental findings.

Another important aspect of the present work concerns the evolution of the physical quantities affected by the presence of the field-induced quantum critical point. In our recent work [12,13], we have shown that the temperature dependence of the magnetic field $H_{\max}$ at which magnetoresistivity has a maximum is a signature of system's proximity to field-induced QCP. Consequently, here we study the dependence of $H_{\max}$ on pressure. We find a remarkable similarity between the dependence of the residual resistivity and $(dH_{\max}/dT)^{-1}$ on pressure. Yet, this result is not surprising because it is well understood that the tendency towards antiferromagnetic ordering originates from the partial screening of the f moments by conduction electrons. Hence, a strong pressure dependence of the relevant physical quantities such as A and $H_{\max}$ is expected.

This paper is organized as follows. In the next section we provide the details of our experimental measurements. The results of our measurements are presented in Sec. III. Section IV is devoted to theoretical modeling of a disordered Kondo lattice under pressure. Specifically, we find that both the residual resistivity and the coefficient in front of the leading temperature-dependent term decrease under pressure, in agreement with our experimental results. In Sec. V we provide the discussion of our results and conclusions.

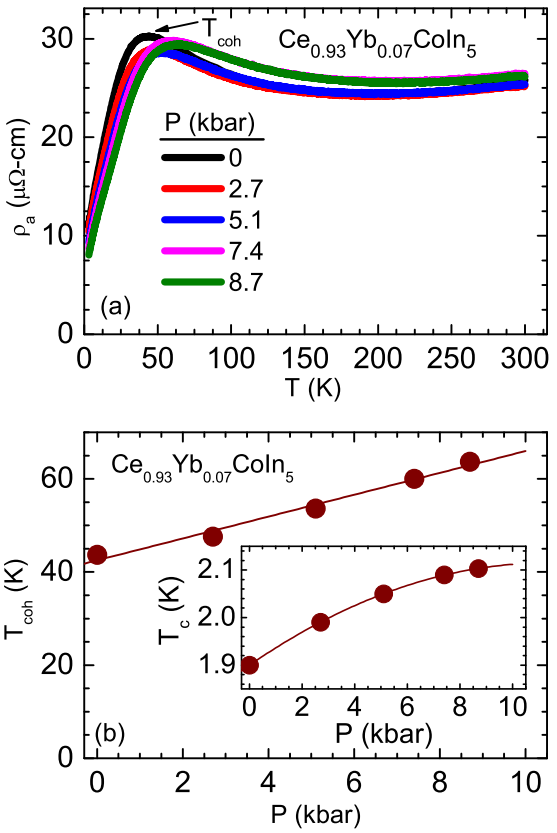

FIG. 1. (Color online) (a) Resistivity ρ_a of $Ce_{0.93}Yb_{0.07}CoIn_5$ as a function of temperature T for different pressures P (0, 2.7, 5.1, 7.4, and 8.7 kbar). The arrow at the maximum of the resistivity data marks the coherence temperature $T_{\rm coh}$. (b) Evolution of $T_{\rm coh}$ as a function of pressure P. Inset: Superconducting critical temperature T_c as a function of pressure P. The solid lines are guides to the eye.

II. EXPERIMENTAL DETAILS

Single crystals of $Ce_{1-x}Yb_xCoIn_5$ were grown using an indium self-flux method. These crystals have a nominal Yb doping $x_{\rm nom} = 0.2$ and an actual doping $x_{\rm act} = 0.07$. The crystal structure and unit cell volume were determined from x-ray powder diffraction measurements, while the actual composition was determined according to the method developed by Jang *et al.* [24]. Since all previous publications on this system give the nominal Yb concentration instead of the actual concentration, in this paper we use the nominal concentrations whenever referring to the results of earlier publications in order to be consistent with their reports, while we use the actual Yb concentration when we refer to the present work. We note that the study by Jang *et al.* [24] has shown that $x_{\rm act} \approx \frac{1}{3}x_{\rm nom}$, providing that the nominal Yb doping is less than about 40%.

The single crystals studied have a typical size of $2.1 \times 1.0 \times 0.16$ mm^3, with the c axis along the shortest dimension of the crystals. They were etched in concentrated HCl for several hours to remove the indium left on the surface during the growth process and were then rinsed thoroughly in ethanol. Four leads were attached to the single crystals, with the current $I \parallel a$ axis, using a silver-based conductive epoxy. We performed resistivity (ρ_a) along the a axis and transverse ($H \perp ab$) magnetoresistivity (MR) measurements as a function of temperature between 2–300 K, applied magnetic field up to 14 T, and applied hydrostatic pressure (P) up to 8.7 kbar.

III. EXPERIMENTAL RESULTS AND DISCUSSION

Figure 1(a) shows ρ_a data as a function of temperature of a $Ce_{0.93}Yb_{0.07}CoIn_5$ single crystal measured under pressure. The qualitative behavior of resistivity is the same for all pressures used in this study: the resistivity initially decreases as the sample is cooled from room temperature, then it passes through a minimum in the temperature range 150–200 K, followed by an increase as the temperature is further lowered. This increase is consistent with a logarithmic temperature dependence, in accordance to the single-ion Kondo effect. With the onset of coherence effects at the Kondo lattice coherence temperature ($T_{\rm coh}$) (defined as the peak in the resistivity data), the resistivity decreases with further decreasing the temperature below $T_{\rm coh}$, while at even lower T, superconductivity sets in at T_c.

The onset of coherence is governed by the process in which the f electrons of Ce can resonantly tunnel into the conduction band, i.e., $f^1 \rightleftharpoons f^0 + e$. Because the cell volume Ω changes due to these resonant processes, i.e., $\Omega(f^1) - \Omega(f^0) > 0$, the electronic properties are strongly susceptible to the application of external pressure. Thus, we expect that pressure increases the local hybridization of $Ce_{0.93}Yb_{0.07}CoIn_5$ and, hence,

increases the coherence temperature (see Sec. IV for the related discussion). Figure 1(b) shows that, indeed, the disordered Kondo lattice T_{coh} increases with increasing pressure, just as it does for pure $CeCoIn_5$ and the other members of the $Ce_{1-x}R_xCoIn_5$ (R = rare-earth) series [22].

The inset to Fig. 1(b) shows the pressure dependence of T_c. For small values of pressures, clearly $T_c \propto T_{coh}$ as they linearly grow with pressure [see Fig. 1(b) and its inset]. This is expected since at low temperatures the coherence temperature of superconducting heavy-fermion metals plays the role of a renormalized bandwidth and, therefore, provides the ultraviolet cutoff for the superconducting instability.

It is well known [25–28] that large and small Fermi surfaces coexist in the stoichiometric $CeCoIn_5$. The quasiparticles from the large Fermi surface are composed of the f states as well as conducting d states due to the hybridization between Ce f and d orbitals, and hence have heavy effective mass. Consequently, the transport and thermodynamic properties of these quasiparticle states strongly depend on pressure since hybridization involves quantum mechanical tunneling between f^0 and f^1 valence states, changing the unit cell volume. In contrast, the quasiparticle states on the small Fermi surface have zero spectral weight contribution from the Ce f states and, therefore, have light effective mass and must show weak pressure dependence. An open question is, do the electrons from the small Fermi surface hybridize with ytterbium ions, or do only the electrons from the large Fermi surface hybridize with both cerium and ytterbium ions? As just discussed, the former (latter) scenario would give a pressure-independent (pressure-dependent) coefficient for the temperature dependence of the scattering processes. Therefore, to address this question, we study the changes in the temperature-dependent part of resistivity under pressure.

As we have already discussed in the Introduction, we have previously shown that there are two distinct contributions to the scattering of the quasiparticles in $Ce_{1-x}Yb_xCoIn_5$ alloys: a $\sqrt{T}$ contribution and a linear-in-T contribution. This latter one is due to quantum critical fluctuations and it is observed only at small Yb doping ($x_{nom} \leqslant 0.2$, $x_{act} \leqslant 0.07$) [see Eq. (1)]. In what follows we trace out the changes in the coefficients A and B with pressure for the $Ce_{0.93}Yb_{0.07}CoIn_5$ alloy, for which both of these contributions are present at least over a certain temperature range and under ambient pressure. The goal is to determine the effect of pressure on quantum critical fluctuations and on the scattering mechanism that gives the $\sqrt{T}$ dependence in resistivity. Figure 2(a) shows that the data are fitted very well with Eq. (1) (the solid lines are the fits to the data) for $3 \leqslant T \leqslant 15$ K and for all pressures studied. From these fits we obtain the pressure dependence of the fitting parameters ρ_{a0}, A, and B, which allow us to probe the relative contribution of heavy- and light-quasiparticle states to scattering.

Figure 2(b) shows the pressure dependence of the parameters A and B extracted from the fitting of $\rho_a(T)$ of Fig. 2(a), which, as discussed above, are the weights of the linear-in-T and square-root-in-T scattering dependences, respectively. Notice that A decreases while B remains relatively constant with increasing pressure. The suppression of A with pressure indicates that the AFM quantum fluctuations are suppressed with increasing pressure. Also, the insensitivity of B to

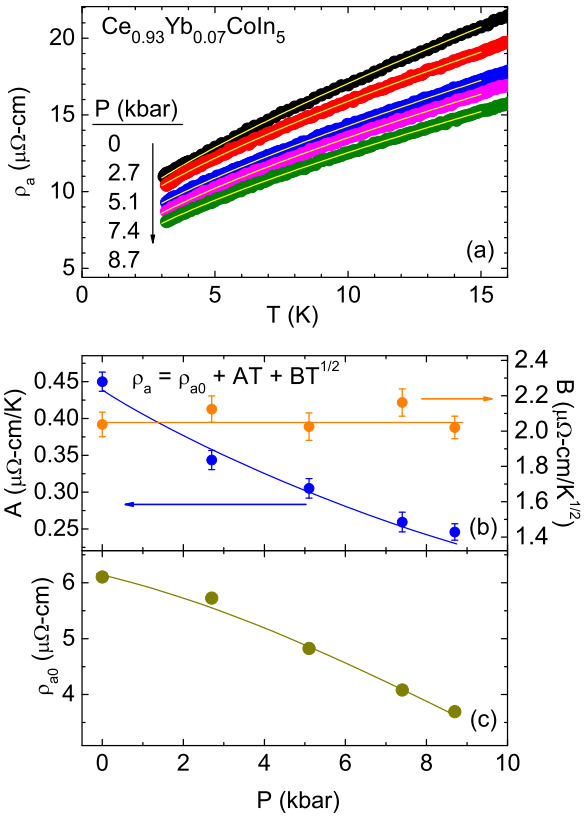

FIG. 2. (Color online) (a) Fits of the resistivity ρ_a data with $\rho_a(P,T) = \rho_{a0}(P) + A(P)T + B(P)\sqrt{T}$ for different pressures for $Ce_{0.93}Yb_{0.07}CoIn_5$ in the temperature range $3\ \text{K} \leqslant T \leqslant 15\ \text{K}$. (b) Pressure P dependence of the linear T contribution A and $\sqrt{T}$ contribution B, obtained from fits of the resistivity data shown in panel (a). (c) Pressure P dependence of the residual resistivity ρ_{a0}, obtained from the fits.

pressure suggests that the inelastic scattering events leading to the $\sqrt{T}$ dependence in this temperature range involve light effective mass quasiparticles from the small Fermi surface. Hence, these $\rho_a(T)$ data for $3 \leqslant T \leqslant 15$ K show that there are two distinct contributions to scattering originating from the two Fermi surfaces: AFM quantum fluctuations of the heavy quasiparticles (with a linear-in-T scattering behavior) and quasiparticles from the small Fermi surface (with a $\sqrt{T}$ scattering behavior).

Moreover, the value of the coefficient $B(P=0,x)$ increases with ytterbium dilution [12] and it remains essentially unchanged under the application of pressure at temperatures well above T_c. These observations strongly suggest that the value of $B(P=0,x)$ is governed by the quasiparticle excitations from the Fermi pockets near the M points of the quasi-two-dimensional Brillouin zone. Recall that according to the recent thermopower measurements and subsequent theoretical studies [28,29] of the parent compound $CeCoIn_5$, the Fermi pockets near the M points remain ungapped giving rise to the nonzero thermal conductivity in the superconducting state. If we now consider the results of the recent penetration depth measurements that show the disappearance of the nodes in the superconducting order parameter for $x_{nom} \approx 0.2$ [17], we conclude that with Yb doping: (i) both Fermi surfaces must

be gapped below T_c due to the proximity pairing effect, and (ii) the absence of the nodes in the superconducting order parameter for $x_{\rm nom} \geqslant 0.2$ suggest that the order parameter may have exotic symmetry, either $d + is$ or $d + id$ [30]. The d component must be present since the order parameter of the parent compound $CeCoIn_5$ has $d_{x^2-y^2}$ symmetry [31,32], while the conventional s-wave superconductivity can be ruled out due to monotonous concentration dependence of T_c. Therefore, intriguingly, $Ce_{1-x}Yb_xCoIn_5$ may provide an important playground for the realization of the long thought topological superconductivity [33]. However, to verify the realization of specific scenarios for the symmetry of the superconducting order parameter in $Ce_{1-x}Yb_xCoIn_5$, one would need a detailed understanding of the electronic properties in both normal and superconducting states [30].

Figure 2(c) shows the pressure dependence of the residual resistivity ρ_0 extracted from the fitting of the data of Fig. 2(a). As discussed in the Introduction, the residual resistivity in this system depends on the impurity concentration in accordance with Nordheim's law. In systems with proximity to a quantum critical point, there will also be a contribution to residual resistivity from the quantum critical fluctuations. Since tuning with pressure does not introduce any impurity scattering in the system, the decrease in residual resistivity with increasing pressure indicates that the scattering due to AFM quantum spin fluctuations is suppressed by pressure, hence the system is driven away from the QCP. Indeed, quantum fluctuations in this family of heavy-fermion superconductors are known to be suppressed by pressure because the AFM order in the Ce lattice is suppressed [34–36].

Figure 3(a) shows ρ_a data vs $\sqrt{T}$ around the superconducting transition temperature ($1.8 \leqslant T \leqslant 5$ K). This figure shows that from just above T_c to about 4 K, the $\rho_a(T)$ data follow very well a $\sqrt{T}$ dependence [solid lines are linear fits to the data with $\rho_a(P,T) = \rho_{a0}(P) + B^*(P)\sqrt{T}$]. The pressure dependence of the coefficient B^* is shown in the inset to Fig. 3. Notice that B^* is significantly suppressed with increasing pressure. This pressure dependence of B^* suggests that the scattering just above T_c is largely governed by fluctuating Cooper pairs originating from the heavy Fermi surface. This observation is in agreement with the fluctuation correction to resistivity due to preformed Cooper pairs composed of heavy quasiparticles. Indeed, for a three-dimensional (3D) Fermi surface and in the case of a strong coupling superconductor with relatively small coherence length [37], one expects a $\sqrt{T}$ fluctuation contribution to resistivity [38]. Therefore, these $\rho_a(T)$ data show that the strong SC fluctuations of the heavy quasiparticles give the $\sqrt{T}$ dependence just above T_c and that the linear-in-T contribution of Eq. (1) that is due to the system's proximity to the field-induced QCP, is masked by these strong SC fluctuations. The superconducting fluctuations, nevertheless, decrease as the system moves away from T_c to higher temperatures. Indeed, as discussed above, the resistivity data reveal that other scattering mechanisms dominate at temperatures above about 4 K [see Fig. 2 and its discussion].

Alternatively, the $\sqrt{T}$ dependence of the resistivity just above T_c is also consistent with the composite pairing theory in a 3D system [39], which predicts an incoherent transport

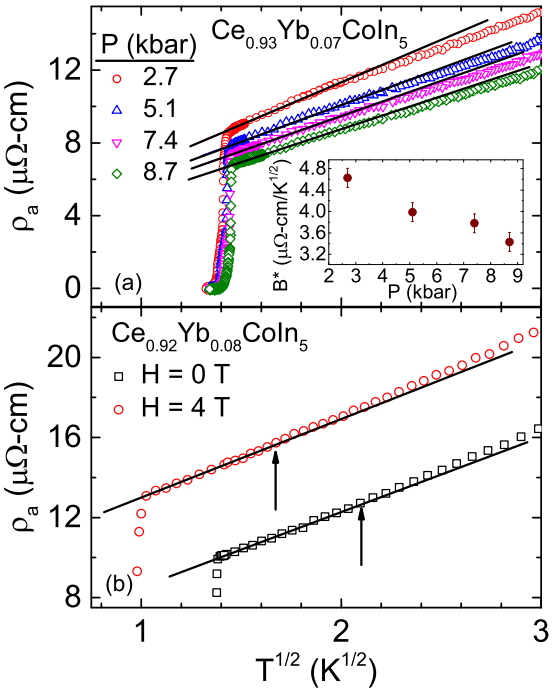

FIG. 3. (Color online) (a) Resistivity ρ_a of $Ce_{0.93}Yb_{0.07}CoIn_5$ as a function of $\sqrt{T}$, in the temperature range $1.8\ {\rm K} \leqslant T \leqslant 5$ K. The solid lines are linear fits of the data with $\rho_a(P,T) = \rho_{a0}(P) + B^*(P)\sqrt{T}$ for $1.8 \leqslant T \leqslant 4$ K. Inset: Pressure P dependence of the coefficient B^*. (b) ρ_a vs $\sqrt{T}$ for $Ce_{0.92}Yb_{0.08}CoIn_5$ measured in zero magnetic field and at 4 T. The 4 T data has been offset upwards by 5 $\mu\Omega$ cm for visual clarity.

of composite Cooper pairs above the superconducting critical temperature with the resistivity growing as $\sqrt{T}$. It is important to emphasize that the size of the composite pairs is only a few lattice spacing, i.e., the electrons in a composite pair are tightly bound. From this point of view, the transport of composite pairs is not governed by fluctuation corrections to conductivity, which are usually discussed in the context of conventional superconductors. Nevertheless, the decrease in B^* with increasing pressure is also consistent with this theory because the composite pairs incorporate the heavy quasiparticles.

Figure 3(b) shows ρ_a data vs $\sqrt{T}$ around the superconducting transition temperature ($1.8 \leqslant T \leqslant 5$ K), measured at ambient pressure in zero magnetic field and 4 T. The temperature at which the data deviate from the $\sqrt{T}$ dependence decreases with applied field, showing that, as expected, the Cooper pair fluctuations are suppressed by magnetic field.

Next, we present the results of transverse ($H \perp ab$) magnetoresistivity (MR) measurements, defined as $\Delta\rho_a/\rho_a(0) \equiv [\rho_a(H) - \rho_a(H=0)]/\rho_a(H=0)$, on $Ce_{0.93}Yb_{0.07}CoIn_5$ in applied magnetic fields up to 14 T, for temperatures ranging from 2–60 K, and applied pressures up to 8.7 kbar. The main panel of Fig. 4 and its inset show such MR curves measured at ambient pressure and 5.1 kbar, respectively. The 9 K MR data in both panels show nonmonotonic H dependence: the MR increases with increases field, displays a maximum at a field $H_{\rm max}$, and decreases with further increasing H, with an H^2 dependence at high fields (see inset to Fig. 4) that is typical of a single-ion

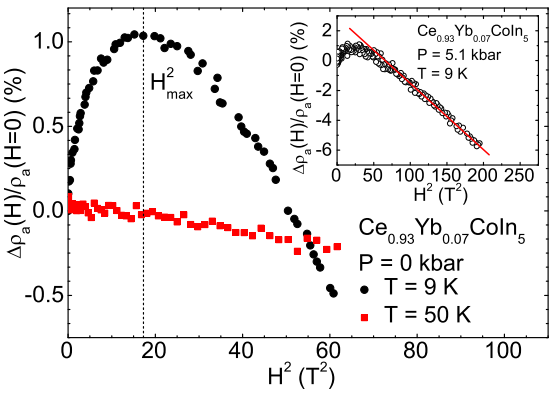

FIG. 4. (Color online) Magnetic field H dependence (plotted as function of H^2) of magnetoresistivity (MR) $\Delta\rho_a/\rho_a(H=0) \equiv [\rho_a(H) - \rho_a(H=0)]/\rho_a(H=0)$ of $Ce_{0.93}Yb_{0.07}CoIn_5$ measured at two different temperatures and ambient pressure. The dashed line in the main figures marks H_{max}, corresponding to the coherence giving way to single-ion Kondo behavior. Inset: MR data vs H^2 measured under 5.1 kbar. The red line shows the quadratic regime of MR.

Kondo system. This positive MR behavior at low H values is due to the formation of the coherent Kondo lattice state. H_{max} represents the value where the coherent state gives way to the single-ion state due to the fact that magnetic field breaks the coherence of the Kondo lattice [40–45].

In a conventional Kondo lattice system, as T increases, H_{max} moves toward lower field values, signifying that a lower field value is sufficient to break coherence at these higher temperatures due to thermal fluctuations, with a complete suppression of the positive contribution to MR, hence $H_{max} = 0$, at $T \approx T_{coh}$ (red solid squares in Fig. 4). On the other hand, as we have recently revealed [12], $H_{max}(T)$ in the $Ce_{1-x}Yb_xCoIn_5$ alloys with concentrations $x_{act} \leqslant 0.07$ shows deviation from the conventional Kondo behavior and exhibits a peak, below which H_{max} decreases with decreasing temperature. This is shown in Fig. 5, which is a plot of the temperature dependence of H_{max} for four different hydrostatic pressures. We have attributed the decrease in $H_{max}(T)$ with decreasing T to quantum spin fluctuations that dominate the MR behavior below about 20 K [12]. Notice that $H_{max}(T)$ shows linear behavior below 10 K (see Fig. 5). A linear extrapolation of this low-T behavior to zero temperature gives H_{QCP} [12]. Notice that $H_{QCP} \approx 0.2$ T in $Ce_{0.93}Yb_{0.07}CoIn_5$ at ambient pressure, as previously reported [12], showing that this Yb doping is close to the quantum critical value x_c for the $Ce_{1-x}Yb_xCoIn_5$ alloys.

Three notable features are revealed by Fig. 5: (i) the application of pressure does not change qualitatively the $H_{max}(T)$ dependence, (ii) there is no noticeable change in the value of H_{QCP} with pressure for $P \leqslant 8.7$ kbar, most likely because of the already small value of H_{QCP} ($H_{QCP} = 0.2$ T) at ambient pressure, and (iii) both the value of H_{max} and the position in T of the $H_{max}(T)$ peak shifts to higher temperatures with increasing pressure; as a result, the slope dH_{max}/dT for $T < 10$ K increases with pressure.

According to Doniach's phase diagram [46], the Kondo temperature T_K and the magnetic exchange interaction temperature T_{RKKY} of Ce Kondo lattice increase with increasing pressure. Hence, the increase in H_{max} with pressure is a result of increased T_{coh}, and the shift in the peak of $H_{max}(T)$ to higher T with pressure is a result of the increase of both T_{RKKY} and T_{coh} with pressure. The increase in the slope dH_{max}/dT with increasing pressure means that a larger applied field is required to break the Kondo singlet. We note that both quantum spin fluctuations and applied magnetic field contribute to the breaking of Kondo coherence at temperatures $T < 10$ K. Therefore, a larger dH_{max}/dT at higher pressures can be understood in terms of weaker quantum spin fluctuations since a larger field is required to break the Kondo singlet compared with the field required for smaller dH_{max}/dT where spin fluctuations are stronger.

We show in Fig. 6 the inverse of this slope as a function of pressure, normalized to its zero pressure value. We also show in the same figure (right vertical axis) the residual resistivity as a function of pressure, also normalized to its zero pressure value. Notice that these two quantities scale very well, indicating that the same physics dominates their behavior with pressure, i.e., the suppression of quantum critical fluctuations with increasing pressure.

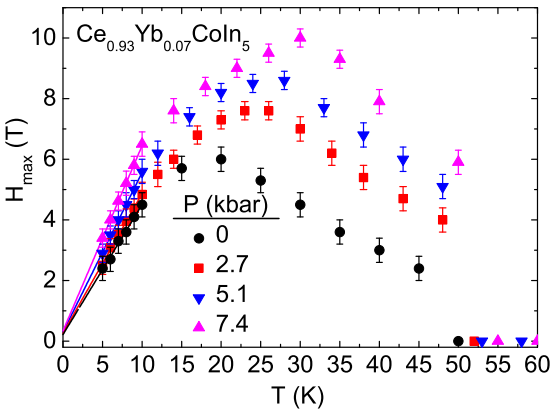

FIG. 5. (Color online) Temperature T dependence of the maximum in magnetoresistivity H_{max} for different pressures P. The solid lines below 10 K are linear fits to the data.

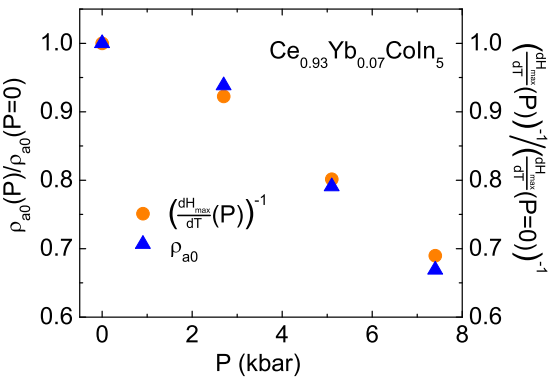

FIG. 6. (Color online) Pressure P dependence of residual resistivity ρ_{a0} (obtained through the fitting of the resistivity data as discussed in the text), normalized to its value at zero pressure (right vertical axis) and P dependence of inverse slope of $H_{max}(T)$ normalized to its value at zero pressure (left vertical axis).

IV. THEORY

In this section, we will formulate a general approach to Kondo alloys diluted with magnetic dopants that will help us to interpret our experimental results. In what follows, we first introduce the model in order to study the effects of pressure in disordered Kondo lattice. Then, we will employ the coherent potential within the mean-field theory for the disordered Kondo lattice to compute the pressure dependence of the Kondo lattice coherence temperature and residual conductivity.

A. Model

We consider the following model Hamiltonian, which we write as a sum of three terms

$$\hat{\mathcal{H}} = \hat{H}_0 + \hat{H}_{Kh} + \hat{H}_V. \tag{2}$$

The first term describes the kinetic energy of the conduction and f electrons in the unperturbed (i.e., spatially homogeneous) Kondo lattice:

$$\hat{H}_0 = \sum_{\mathbf{k}\sigma} \epsilon_{\mathbf{k}} \hat{c}^\dagger_{\mathbf{k}\sigma} \hat{c}_{\mathbf{k}\sigma} + \sum_{\mathbf{k}\sigma} \varepsilon_f \hat{f}^\dagger_{\mathbf{k}\sigma} \hat{f}_{\mathbf{k}\sigma}\,, \tag{3}$$

where $\epsilon_{\mathbf{k}} = -(t_c/2)(\cos k_x + \cos k_y) - \mu_c$ is the single-particle energy taken relative to the chemical potential μ_c (here we will ignore the transport along the z axis). The second term in Eq. (2) accounts for the Kondo holes, i.e., it prohibits the f electrons from occupying an impurity site, and it also describes the impurity f electrons denoted by $\hat{p}$:

$$\begin{aligned}\hat{H}_{Kh} = &\sum_{i\sigma}(1-\xi_i)(\varepsilon_{0f}+\varepsilon_f)\hat{f}^\dagger_{i\sigma}\hat{f}_{i\sigma} + \sum_\sigma \tilde{\epsilon}_f \hat{p}^\dagger_\sigma \hat{p}_\sigma \\ &+ \frac{U_f}{2}\sum_{i\sigma}\xi_i \hat{f}^\dagger_{i\uparrow}\hat{f}_{i\uparrow}\hat{f}^\dagger_{i\downarrow}\hat{f}_{i\downarrow} + U_p \hat{p}^\dagger_\uparrow \hat{p}_\uparrow \hat{p}^\dagger_\downarrow \hat{p}_\downarrow\,,\end{aligned} \tag{4}$$

where summation goes over all lattice cites, and

$$\xi_i = \begin{cases} 0, & i = 0 \\ 1, & i \neq 0 \end{cases}, \tag{5}$$

with $i = 0$ denoting the position of an impurity site. The first term in Eq. (4) accounts for an f-electron state on an impurity site. Physically, this process cannot happen. Therefore, at the end of the calculation, the energy of the f electron on the impurity site will be taken to infinity, $\varepsilon_{0f} \to \infty$, to ensure $\langle \hat{f}^\dagger_{i=0\sigma}\hat{f}_{i=0\sigma}\rangle = 0$. Lastly, the third term in Eq. (2) accounts for the hybridization between the conduction electrons and both cerium f electrons and ytterbium f holes:

$$\hat{H}_V = \sum_{i\sigma}\xi_i(V_f \hat{c}^\dagger_{i\sigma}\hat{f}_{i\sigma} + \text{H.c.}) + \sum_{\mathbf{k}\sigma}(V_p \hat{c}^\dagger_{\mathbf{k}\sigma}\hat{p}_\sigma + \text{H.c.}). \tag{6}$$

Clearly, the theoretical analysis of this model is hindered by the presence of the Hubbard interaction terms with both U_f and U_p being the largest energy scales in the problem. To make progress, we will adopt the slave-boson mean-field theory (SBMF) approach. Thus, we will set U_f and U_p to infinity:

$$U_f \to \infty\,, \quad U_p \to \infty. \tag{7}$$

The double occupancy on the f sites is excluded by introducing the slave-boson projection operators:

$$\begin{aligned}&\hat{f}_{i\sigma} \to \hat{b}^\dagger_i \hat{f}_{i\sigma}\,, \quad \hat{f}^\dagger_{i\sigma} \to \hat{f}^\dagger_{i\sigma}\hat{b}_i\,, \\ &\hat{p}_\sigma \to \hat{a}^\dagger \hat{p}_\sigma\,, \quad \hat{p}^\dagger_\sigma \to \hat{p}^\dagger_\sigma \hat{a},\end{aligned} \tag{8}$$

supplemented by the following constraint conditions:

$$\sum_\sigma \hat{f}^\dagger_{i\sigma}\hat{f}_{i\sigma} + \hat{b}^\dagger_i \hat{b}_i = 1, \quad \sum_\sigma \hat{p}^\dagger_\sigma \hat{p}_\sigma + \hat{a}^\dagger\hat{a} = 1. \tag{9}$$

Thus, the phase space is reduced to the set of either singly occupied states $|b^0 f^1\rangle$ or empty states $|b^1 f^0\rangle$ for the f electrons and, similarly, $|a^0 p^1\rangle$ or $|a^1 p^0\rangle$ for f holes. Clearly, the hybridization part of the Hamiltonian in Eq. (6) always acts only between these two states. Thus, for the kinetic energy terms, we find

$$\hat{f}^\dagger_{i\sigma}\hat{f}_{i\sigma}|b^0 f^1\rangle \to \hat{f}^\dagger_{i\sigma}\hat{b}_i\hat{b}^\dagger_i\hat{f}_{i\sigma}|b^0 f^1\rangle = \hat{f}^\dagger_{i\sigma}\hat{f}_{i\sigma}|b^0 f^1\rangle. \tag{10}$$

In the mean-field approximation, the projection (slave-boson) operators are replaced with their expectation values:

$$\hat{b}_i \to \langle \hat{b}_i\rangle = b\,, \quad \hat{a} \to \langle \hat{a}\rangle = a. \tag{11}$$

The corresponding mean-field Hamiltonian is

$$\begin{aligned}\hat{\mathcal{H}}_{mf} = &\sum_{\mathbf{k}\sigma}\epsilon_{\mathbf{k}}\hat{c}^\dagger_{\mathbf{k}\sigma}\hat{c}_{\mathbf{k}\sigma} + \sum_{\mathbf{k}\sigma}\varepsilon_f \hat{f}^\dagger_{\mathbf{k}\sigma}\hat{f}_{\mathbf{k}\sigma} \\ &+ \sum_{i\sigma}(1-\xi_i)(\varepsilon_{0f}-\varepsilon_f)\hat{f}^\dagger_{i\sigma}\hat{f}_{i\sigma} + \sum_\sigma \tilde{\epsilon}_f \hat{p}^\dagger_\sigma\hat{p}_\sigma \\ &+ \sum_{i\sigma}\xi_i(V_f b^* \hat{c}^\dagger_{i\sigma}\hat{f}_{i\sigma} + \text{H.c.}) + \\ &+ \sum_{\mathbf{k}\sigma}(V_p a^* \hat{c}^\dagger_{\mathbf{k}\sigma}\hat{p}_\sigma + \text{H.c.}) \\ &+ \sum_i \xi_i \lambda_b \left(\sum_\sigma \hat{f}^\dagger_{i\sigma}\hat{f}_{i\sigma} + |b|^2 - 1\right) \\ &+ \lambda_a\left(\sum_\sigma \hat{p}^\dagger_\sigma\hat{p}_\sigma + |a|^2 - 1\right),\end{aligned} \tag{12}$$

where $\lambda_{a,b}$ are Lagrange multipliers, which will be computed self-consistently. Let us introduce the following parameters:

$$E_f = \lambda_b + \varepsilon_f\,, \quad E_{0f} = \varepsilon_{0f} - E_f\,, \quad \epsilon_f = \tilde{\epsilon}_f + \lambda_a. \tag{13}$$

In addition, we introduce $z = 1 - x$ with x being the concentration of Yb ions:

$$z = \frac{1}{N_s}\sum_i \xi_i. \tag{14}$$

In this expression N_s is the total number of sites. After rearranging the terms in Eq. (12) and using Eq. (13) we obtain:

$$\begin{aligned}&\hat{\mathcal{H}}_{mf} = \hat{H}^{(b)}_{mf} + \hat{H}^{(a)}_{mf}\,, \\ &\hat{H}^{(b)}_{mf} = \sum_{\mathbf{k}\sigma}\epsilon_{\mathbf{k}}\hat{c}^\dagger_{\mathbf{k}\sigma}\hat{c}_{\mathbf{k}\sigma} + \sum_{\mathbf{k}\sigma}E_f\hat{f}^\dagger_{\mathbf{k}\sigma}\hat{f}_{\mathbf{k}\sigma} + E_{0f}\hat{f}^\dagger_{0\sigma}\hat{f}_{0\sigma} \\ &\qquad + \sum_{i\sigma}\xi_i(V_f b^*\hat{c}^\dagger_{i\sigma}\hat{f}_{i\sigma} + b\hat{f}^\dagger_{i\sigma}\hat{c}_{i\sigma}) + zN_s\lambda_b(|b|^2 - 1),\end{aligned}$$

$$\hat{H}^{(a)}_{mf} = \sum_{\sigma} \epsilon_f \hat{p}^{\dagger}_{\sigma} \hat{p}_{\sigma} + V_p \sum_{\mathbf{k}\sigma} (a^* \hat{c}^{\dagger}_{\mathbf{k}\sigma} \hat{p}_{\sigma} + a \hat{p}^{\dagger}_{\sigma} \hat{c}_{\mathbf{k}\sigma}) + \lambda_a (|a|^2 - 1). \quad (15)$$

Because ytterbium ions are in the mixed valence state, the hybridization amplitude $V_p \ll V_f$. Moreover, we assume that the condensation temperature T_{Yb} for the bosons a is significantly smaller than the Ce Kondo lattice coherence temperature T_{coh}. This assumption is justified by the similarity in the physical properties of the Yb ion in $Yb_xY_{1-x}InCu_4$ and in $Ce_{1-x}Yb_xCoIn_5$: the ytterbium valence state is close to Yb^{3+} for $x_{\mathrm{nom}} \ll 0.1$ and becomes $Yb^{2.5+}$ for $x_{\mathrm{nom}} \sim 0.1$. At the same time, in $Yb_xY_{1-x}InCu_4$, for small x, the single site Kondo temperature is approximately 2 K [47]. Thus, in our choice of the bare model parameters, we must keep in mind that the condensation temperature for the a bosons is lower than the one for the b bosons, $T_{\mathrm{Yb}} < T_{\mathrm{coh}}$.

B. Coherent potential approximation

To analyze the transport properties of the disordered Kondo lattice, we employ the coherent potential approximation (CPA) [23,48–51]. The idea of the CPA is to introduce an effective medium potential, which allows for an equivalent description of the disordered system. In particular, the effective potential is considered to be purely dynamical. This approximation is valid when the scattering events on different impurity sites are independent.

To formulate the CPA, we introduce the Lagrangian for the disordered Kondo lattice (which is related to $\hat{H}^{(b)}_{mf}$):

$$\mathcal{L} = \sum_{\mathbf{k}\sigma} [\hat{c}^{\dagger}_{\mathbf{k}\sigma}(\partial_\tau + \epsilon_{\mathbf{k}})\hat{c}_{\mathbf{k}\sigma} + \hat{f}^{\dagger}_{\mathbf{k}\sigma}(\partial_\tau + E_f)\hat{f}_{\mathbf{k}\sigma}] + \sum_{\sigma} \hat{f}^{\dagger}_{0\sigma}(\partial_\tau + E_f)\hat{f}_{0\sigma} + zN_s\lambda_b(|b|^2 - 1) + \sum_{i\sigma} \xi_i (V_f b^* \hat{c}^{\dagger}_{i\sigma} \hat{f}_{i\sigma} + b \hat{f}^{\dagger}_{i\sigma} \hat{c}_{i\sigma}), \quad (16)$$

where, for brevity, we omit the dependence of the fermionic fields on Matsubara time τ. Note that we have not included the terms that involve p fermions. The reason is that the p fermions can be formally integrated out, which will lead to the appearance of the self-energy correction $\Sigma_a(\tau - \tau')$ in the first term of Eq. (16). However, to keep our expressions compact, we will include this term later when we analyze the transport properties. Within the frame of the CPA, we introduce an effective medium Lagrangian for the disordered Kondo lattice system as follows:

$$\mathcal{L}_{\mathrm{eff}} = \int_0^{\beta} d\tau' \sum_{\mathbf{k}\sigma} \hat{\psi}^{\dagger}_{\mathbf{k}\sigma}(\tau) \begin{bmatrix} \delta(\tau - \tau')(\partial_\tau + \epsilon_{\mathbf{k}}) + S_{cc}(\tau - \tau', z) & S_{cf}(\tau - \tau', z) \\ S_{fc}(\tau - \tau', z) & \delta(\tau - \tau')(\partial_\tau + E_f) + S_{ff}(\tau - \tau', z) \end{bmatrix} \hat{\psi}_{\mathbf{k}\sigma}(\tau') + zN_s\lambda_b(|b|^2 - 1), \quad (17)$$

where $\beta = 1/k_B T$, we introduced the two-component spinor $\hat{\psi}^{\dagger}_{\mathbf{k}\sigma} = (\hat{c}^{\dagger}_{\mathbf{k}\sigma}\ \hat{f}^{\dagger}_{\mathbf{k}\sigma})$ for brevity, and $S_{ab}(\tau, z)$ are the components of the coherent potential that we will have to determine self-consistently. The self-consistency condition for the components of $S_{ab}(\tau, z)$ is obtained by requiring that the corresponding correlation functions for the effective Lagrangian, Eq. (17), are equal to the disorder-averaged correlators for the disordered Kondo lattice, Eq. (16) [48]. In the Kondo hole limit ($E_{0f} \to \infty$), it follows:

$$\hat{S}(i\omega_n, z) = \begin{pmatrix} 0 & bV_f \\ b^*V_f & S_{ff}(i\omega_n, z) \end{pmatrix}, \quad (18)$$

where $i\omega_n = \pi T(2n + 1)$ is a fermionic Matsubara frequency and

$$S_{ff}(\omega, x)F_{ff}(\omega) = z - 1, \qquad F_{ff}(\omega) = \sum_{\mathbf{k}} \frac{\omega - \epsilon_{\mathbf{k}}}{(\omega - \epsilon_{\mathbf{k}})(\omega - E_f - S_{ff}(\omega, z)) - V_f^2|b|^2}. \quad (19)$$

These equations allow us to compute the remaining component of the coherent potential (18). $S_{ff}(i\omega, z)$ is a function of parameters E_f and b, which will have to be computed self-consistently by minimizing the free energy.

C. Slave-boson mean-field theory for disordered Kondo lattice under hydrostatic pressure

In order to study the effects of pressure in a disordered Kondo lattice, we need to express the change in the total volume of the system with the corresponding changes in the valence states of Ce and Yb ions. For the Ce ions, the change in the f-shell occupation is positive due to its electronic nature, so that the resonance scattering involves a zero-energy boson, with amplitude b, and an electron: $f^{n+1}(j,m) \rightleftharpoons f^n(j,m) + e^-$. In contrast, for the Yb ions, the resonance scattering involves a zero-energy boson, with amplitude a, and a hole: $f^{n-1}(j,m) \rightleftharpoons f^n(j,m) + e^+$. Thus, for the total volume of the system within the slave-boson mean-field theory, we write [23]:

$$\Omega_t = (1 - z)[\Omega_{0\mathrm{Yb}} + (1 - a^2)\delta\Omega_{\mathrm{Yb}}] + z[\Omega_{0\mathrm{Ce}} + (1 - b^2)\delta\Omega_{\mathrm{Ce}}], \quad (20)$$

where $\Omega_{0\mathrm{Yb,Ce}}$ are the cell volumes for the singlet (nonmagnetic) states on Yb (f^{14}) and Ce (f^0) ions, correspondingly. Moreover, $\delta\Omega_{\mathrm{Yb,Ce}}$ account for the difference in cell volumes between two f-ion configurations. Note that $\delta\Omega_{\mathrm{Yb}} < 0$ while $\delta\Omega_{\mathrm{Ce}} > 0$.

To obtain the self-consistency equations for the slave-boson amplitude b and constraint variable λ_b, we define the grand

canonical enthalpy for an alloy under pressure P:

$$K = -k_B T \log Z_{\rm eff}\,, \qquad Z_{\rm eff} = {\rm Tr}\{e^{-\int_0^\beta d\tau \mathcal{L}_{\rm eff}(\tau) - P\Omega_t}\}. \tag{21}$$

Minimizing the enthalpy with respect to b and λ_b, we obtain:

$$z(b^2-1) + 2T\sum_{i\omega_n} F_{ff}(i\omega_n) = 0\,, \qquad zb(\lambda_b - P\delta\Omega_{\rm Ce}) + 2V_f T\sum_{i\omega_n} F_{fc}(i\omega_n) = 0\,, \tag{22}$$

where $i\omega_n = i\pi T(2n+1)$ are Matsubara frequencies and

$$F_{fc}(\omega) = bV_f \sum_{\mathbf{k}} \frac{1}{(\omega-\epsilon_{\mathbf{k}})[z - E_f - S_{ff}(\omega,z)] - V_f^2|b|^2}. \tag{23}$$

In addition, the third equation is the conservation of the total number of particles $N_{\rm tot} = n_c + z n_f$, with

$$n_c = T\sum_{i\omega_n}\sum_{\mathbf{k}} e^{i\omega_n 0+} G_{cc}(\mathbf{k}, i\omega_n), \qquad G_{cc}(\mathbf{k},\omega) = \frac{\omega - E_f - S_{ff}(\omega,z)}{(\omega-\epsilon_{\mathbf{k}})(\omega - E_f - S_{ff}(\omega,z)) - V_f^2|b|^2 - \frac{V_p^2 a^2}{\omega-\epsilon_f}}, \tag{24}$$

which allows us to determine the renormalized position of the chemical potential μ_c. We note that equations that determine the value of a and λ_a can be obtained in the same manner as the ones above.

As a result, we find that the slave-boson amplitude b grows linearly with pressure [23], $b \propto P\delta\Omega_t$, see Fig. 7. Also, our analysis of the mean-field equations (22) in the limit $b \to 0$ shows that the Kondo lattice coherence temperature $T_{\rm coh}$ also grows with pressure almost linearly (Fig. 7 inset):

$$T_{\rm coh} \simeq E_f(T_{\rm coh}) \propto P\delta\Omega_t, \tag{25}$$

which is in agreement with our experimental observations [see Fig. 1(b)]. In addition, as expected, we find that (i) both slave-boson amplitude and coherence temperature decrease as the concentration of ytterbium atoms increases, and (ii) the presence of the ytterbium f electrons leads to a small reduction in the value of $b(P)$ relative to the case when $a = 0$.

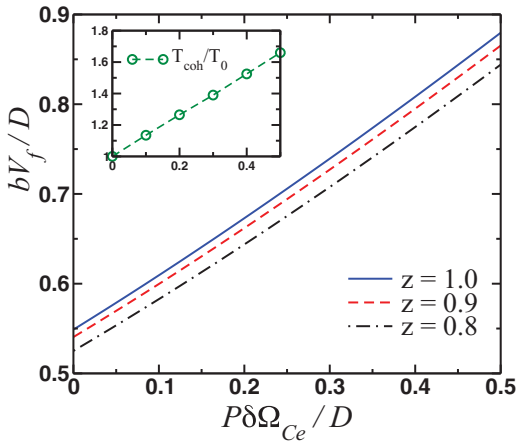

FIG. 7. (Color online) Pressure P dependence of the slave-boson amplitude and coherence temperature $T_{\rm coh}$ (inset) for various concentrations z of the impurity f sites. The dependence of the coherence temperature $T_{\rm coh}$ on pressure for $z = 0.93$ is shown.

D. Transport properties

In this section we discuss the pressure dependence of the residual resistivity of the disordered Kondo lattice described by the Hamiltonian (12). We compute conductivity using the following expression [52]:

$$\sigma_{\alpha\beta}(i\Omega) = \frac{1}{\Omega}[\Pi_{\alpha\beta}(i\Omega) - \Pi_{\alpha\beta}(0)], \tag{26}$$

where $\alpha,\beta = x,y$, $s_\alpha = \sin k_\alpha$, v_F is a Fermi velocity of the heavy quasiparticles, and

$$\Pi_{\alpha\beta}(i\Omega) = e^2 v_F^2 T\sum_{i\omega_n}\sum_{\mathbf{k}} s_\alpha G_{cc}(\mathbf{k}, i\omega_n + i\Omega) s_\beta G_{cc}(\mathbf{k}, i\omega_n). \tag{27}$$

To obtain the dependence of conductivity on the real frequency, we will perform the analytic continuation from $\Omega_n = 2\pi T n > 0$ to real frequencies $i\Omega_n \to \omega$. The residual resistivity can be computed from $\rho_0 = \sigma^{-1}(\omega \to 0)$. We present our results in Fig. 8. In agreement with our experimental results, we find that the residual resistivity decreases with pressure, which is consistent with the suppression of the f-electron density of states [23].

At ambient pressure, the residual resistivity grows linearly with ytterbium concentration, which is again expected given our CPA approximation.

The temperature dependence of resistivity can also be obtained from Eq. (26). Naturally, we find a square-T dependence: $\rho(P,T;z) = \rho_0(P,z) + A_{FL}(P,z)T^2$. Because $A_{FL}(P,z)$ decreases with pressure, as does the coefficient in front of the linear-in-T term in Eq. (1), we conclude that the inelastic scattering of heavy quasiparticles determines the value of $A(P,z)$.

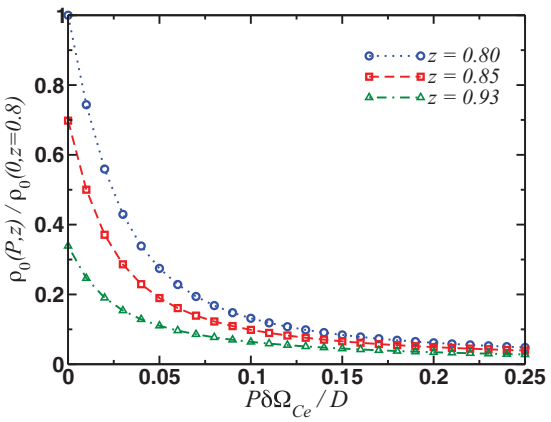

FIG. 8. (Color online) Pressure P dependence of the residual resistivity ρ_0 for various alloy concentrations z.

V. CONCLUSIONS

In this paper, we studied the $Ce_{0.93}Yb_{0.07}CoIn_5$ alloy ($x_{nom} = 0.2$) using transport and magnetotransport measurements under hydrostatic pressure. Our resistivity data reveal that the scattering close to T_c follows a $\sqrt{T}$ dependence, consistent with the composite pairing theory in a 3D system [39] or with a fluctuation correction, with a coefficient that decreases with increasing pressure. This latter result implies that the scattering in this T range is largely governed by the heavy quasiparticles from the heavy Fermi surface, hence it may reflect the scattering of composite pairs [39] as a result of superconducting fluctuations. At higher T, our data reveal the presence of two scattering mechanisms: one linear in T with a coefficient A that decreases with increasing pressure and the other one with a $\sqrt{T}$ dependence with a coefficient B that is pressure independent. Given that the strong pressure dependence of the A parameter directly relates to the strongly hybridized conduction and cerium f-electron states, we believe that the linear temperature dependence of the resistivity is governed by the scattering of heavy quasiparticles, while the scattering processes leading to the $\sqrt{T}$ term in resistivity are governed by the scattering of light electrons from the small Fermi surface. Since the linear T dependence is a result of quantum spin fluctuations, the decrease of A with increasing pressure implies that quantum fluctuations are suppressed with pressure. This conclusion is confirmed by the fact that residual resistivity also decreases with pressure.

We also performed magnetoresistivity measurements under applied hydrostatic pressure in order to study the evolution of quantum critical spin fluctuations with pressure. First, our magnetoresistivity data reveal that this $Ce_{0.93}Yb_{0.07}CoIn_5$ alloy is close to the quantum critical value x_c for the $Ce_{1-x}Yb_xCoIn_5$ alloys. Second, these data confirm our findings from resistivity measurements that quantum critical fluctuations are suppressed with increasing pressure. Finally, we also analyzed the temperature and pressure dependence of the magnetic field H_{max} at which magnetoresistivity reaches its maximum value. At low temperatures, H_{max} grows linearly with temperature. Interestingly, we find that the slope dH_{max}/dT also grows with applied pressure, similar to the dependence on pressure of the coherence temperature. This result suggests that the magnetoresistivity is largely governed by the heavy electrons from the large Fermi surface.

Our theoretical analysis of the disordered Kondo lattice model with magnetic disorder ions shows that despite the presence of magnetic impurities rather than Kondo holes, the coherence temperature grows and residual resistivity decreases with pressure as expected for electronlike Kondo ions [23]. The growth of the coherence temperature leads to the corresponding growth of the superconducting critical temperature, indicating that superconductivity originates predominantly from the heavy Fermi surface.

ACKNOWLEDGMENTS

M.D. thanks Instituto Superior Téchnico (Lisboa, Portugal), where part of this work has been completed, for hospitality. This work was supported by the National Science Foundation (Grant No. NSF DMR-1006606) and Ohio Board of Regents (Grant No. OBR-RIP-220573) at KSU, and by the US Department of Energy (Grant No. DE-FG02-04ER46105) at UCSD.

[1] C. Petrovic, P. G. Pagliuso, M. F. Hundley, R. Movshovich, J. L. Sarrao, J. D. Thompson, Z. Fisk, and P. Monthoux, J. Phys. Condens. Matter **13**, L337 (2001).
[2] J. L. Sarrao and J. D. Thompson, J. Phys. Soc. Jpn. **76**, 051013 (2007).
[3] P. Coleman, *Heavy Fermions: Electrons at the Edge of Magnetism* (Wiley, New York, 2007).
[4] M. Dzero, K. Sun, V. Galitski, and P. Coleman, Phys. Rev. Lett. **104**, 106408 (2010).
[5] M. Z. Hasan and C. L. Kane, Rev. Mod. Phys. **82**, 3045 (2010).
[6] S. Wolgast, C. Kurdak, K. Sun, J. W. Allen, D.-J. Kim, and Z. Fisk, Phys. Rev. B **88**, 180405 (2013).
[7] D. J. Kim, S. Thomas, T. Grant, J. Botimer, Z. Fisk, and J. Xia, Sci. Rep. **3**, 3150 (2013).
[8] X. Zhang, N. P. Butch, P. Syers, S. Ziemak, R. L. Greene, and J. Paglione, Phys. Rev. X **3**, 011011 (2013).
[9] D.-J. Kim, J. Xia, and Z. Fisk, Nature Mater. **13**, 466 (2014).
[10] L. Shu, R. E. Baumbach, M. Janoschek, E. Gonzales, K. Huang, T. A. Sayles, J. Paglione, J. O'Brien, J. J. Hamlin, D. A. Zocco *et al.*, Phys. Rev. Lett. **106**, 156403 (2011).
[11] J. Paglione, T. A. Sayles, P. C. Ho, J. R. Jeffries, and M. B. Maple, Nature Phys. **3**, 703 (2007).
[12] T. Hu, Y. P. Singh, L. Shu, M. Janoschek, M. Dzero, M. B. Maple, and C. C. Almasan, Proc. Natl. Acad. Sci. USA **110**, 7160 (2013).
[13] Y. P. Singh, D. J. Haney, X. Y. Huang, I. K. Lum, B. D. White, M. Dzero, M. B. Maple, and C. C. Almasan, Phys. Rev. B **89**, 115106 (2014).
[14] Y. Onuki, T. Hirai, T. Kumazawa, T. Komatsubara, and Y. Oda, J. Phys. Soc. Jpn. **56**, 1454 (1987).
[15] J. P. Kappler, G. Krill, M. F. Ravet, M. J. Besnus, and M. Meyer, *Valence Fluctuations in Solids: Santa Barbara Institute for Theoretical Physics Conferences, Santa Barbara, California, January 27–30, 1981* (North-Holland, Amsterdam 1981).
[16] A. Polyakov, O. Ignatchik, B. Bergk, K. Götze, A. D. Bianchi, S. Blackburn, B. Prévost, G. Seyfarth, M. Côté, D. Hurt *et al.*, Phys. Rev. B **85**, 245119 (2012).
[17] H. Kim, M. A. Tanatar, R. Flint, C. Petrovic, R. Hu, B. D. White, I. K. Lum, M. B. Maple, and R. Prozorov, Phys. Rev. Lett. **114**, 027003 (2015).
[18] C. M. Varma, Rev. Mod. Phys. **48**, 219 (1976).
[19] G. R. Stewart, Rev. Mod. Phys. **56**, 755 (1984).
[20] C. H. Booth, T. Durakiewicz, C. Capan, D. Hurt, A. D. Bianchi, J. J. Joyce, and Z. Fisk, Phys. Rev. B **83**, 235117 (2011).
[21] L. Dudy, J. D. Denlinger, L. Shu, M. Janoschek, J. W. Allen, and M. B. Maple, Phys. Rev. B **88**, 165118 (2013)

[22] B. D. White, J. J. Hamlin, K. Huang, L. Shu, I. K. Lum, R. E. Baumbach, M. Janoschek, and M. B. Maple, Phys. Rev. B **86**, 100502 (2012).
[23] S. Zhang, Phys. Rev. B **65**, 064407 (2002).
[24] S. Jang, B. White, I. Lum, H. Kim, M. Tanatar, W. Straszheim, R. Prozorov, T. Keiber, F. Bridges, L. Shu *et al.*, Philos. Mag. **94**, 4219 (2014).
[25] A. Koitzsch, T. K. Kim, U. Treske, M. Knupfer, B. Büchner, M. Richter, I. Opahle, R. Follath, E. D. Bauer, and J. L. Sarrao, Phys. Rev. B **88**, 035124 (2013).
[26] T. Maehira, T. Hotta, K. Ueda, and A. Hasegawa, J. Phys. Soc. Jpn. **72**, 854 (2003).
[27] R. Settai, H. Shishido, S. Ikeda, Y. Murakawa, M. Nakashima, D. Aoki, Y. Haga, H. Harima, and Y. Onuki, J. Phys. Condens. Matter **13**, L627 (2001).
[28] V. Barzykin and L. P. Gor'kov, Phys. Rev. B **76**, 014509 (2007).
[29] M. A. Tanatar, J. Paglione, S. Nakatsuji, D. G. Hawthorn, E. Boaknin, R. W. Hill, F. Ronning, M. Sutherland, L. Taillefer, C. Petrovic *et al.*, Phys. Rev. Lett. **95**, 067002 (2005).
[30] M. Dzero (unpublished).
[31] W. K. Park, J. L. Sarrao, J. D. Thompson, and L. H. Greene, Phys. Rev. Lett. **100**, 177001 (2008).
[32] W. K. Park and L. H. Greene, J. Phys. Condens. Matter **21**, 103203 (2009).
[33] X.-L. Qi and S.-C. Zhang, Rev. Mod. Phys. **83**, 1057 (2011).
[34] D. Jaccard, K. Behnia, and J. Sierro, Phys. Lett. A **163**, 475 (1992).
[35] F. Grosche, S. Julian, N. Mathur, and G. Lonzarich, Physica B (Amsterdam, Neth.) **223–224**, 50 (1996).
[36] T. Hu, H. Xiao, T. A. Sayles, M. Dzero, M. B. Maple, and C. C. Almasan, Phys. Rev. Lett. **108**, 056401 (2012).
[37] L. DeBeer-Schmitt, C. D. Dewhurst, B. W. Hoogenboom, C. Petrovic, and M. R. Eskildsen, Phys. Rev. Lett. **97**, 127001 (2006).
[38] M. Tinkham, *Introduction to Superconductivity*, Dover Books on Physics Series (Dover Publications, Mineola, 2012).
[39] O. Erten, R. Flint, and P. Coleman, Phys. Rev. Lett. **114**, 027002 (2015).
[40] P. T. Coleridge, J. Phys. F **17**, L79 (1987).
[41] J. Ruvalds and Q. G. Sheng, Phys. Rev. B **37**, 1959 (1988).
[42] J. Flouquet, P. Haen, F. Lapierre, C. Fierz, A. Amato, and D. Jaccard, J. Magn. Magn. Mater. **76-77**, 285 (1988).
[43] U. Rauchschwalbe, F. Steglich, A. de Visser, and J. Franse, J. Magn. Magn. Mater. **63-64**, 347 (1987).
[44] M. C. Aronson, J. D. Thompson, J. L. Smith, Z. Fisk, and M. W. McElfresh, Phys. Rev. Lett. **63**, 2311 (1989).
[45] F. J. Ohkawa, Phys. Rev. Lett. **64**, 2300 (1990).
[46] S. Doniach, Physica B+C (Amsterdam) **91**, 231 (1977).
[47] M. Očko, J. L. Sarrao, I. Aviani, D. Drobac, I. Živković, and M. Prester, Phys. Rev. B **68**, 075102 (2003).
[48] B. Velický, S. Kirkpatrick, and H. Ehrenreich, Phys. Rev. **175**, 747 (1968).
[49] F. Brouers and A. V. Vedyayev, Phys. Rev. B **5**, 348 (1972).
[50] Z.-Z. Li, Y. Qiu, and W. Xu, Phys. Lett. A **131**, 466 (1988).
[51] Z.-z. Li and Y. Qiu, Phys. Rev. B **43**, 12906 (1991).
[52] G. Mahan, *Many-Particle Physics*, Physics of Solids and Liquids (Springer, Berlin, 2000).